Original Article

Constructing Multiwavelet-based Shearlets and using Them for Automatic Segmentation of Noisy Brain Images Affected by COVID-19

Nasser Aghazadeh, Paria Moradi, Parisa Noras

Department of Applied Mathematics, Azarbaijan Shahid Madani University, Tabriz, Iran

Abstract

Backgorund: Nowadays, everybody's life is dominated by COVID-19, which might have been the source of severe acute respiratory syndrome coronavirus 2. This virus disrupts the lungs first of all. Recently, it has been found that coronavirus may affect the brain. Because all body actions rely on the brain, hence investigating its healthy is an essential item in coronavirus effects. **Method:** Brain image segmentation can be helpful in the detection of the regions damaged by the effects of coronavirus. Since every image given by photography devices may have noises, therefore, first of all, the brain magnetic resonance angiography (MRA) images must be denoised for best investigation. In the present paper, we have presented the construction of multishearlets based on multiwavelets for the first time and have used them for the purpose of denoising. Multiwavelets have some advantages to wavelets. Therefore, we have used them in the shearlet system to expand the properties of multiwavelets in all directions. After denoising, we have proposed a scheme for the automatic characterization of the initial curve in the active contour model for segmentation. Detecting the initial curve is a challenging task in active contour-based segmentation because detecting an initial curve far from the desired region can lead to unfavorable results. **Results:** The results show the performance of using multishearlets in detecting affected regions by COVID-19. Using multishearlets has led to the high value of peak signal-to-noise ratio and Structural similarity index measure in comparison with original shearlets. Original shearlets are constructed from wavelets whereas we have constructed multishearlets from multiwavelets. **Conclusion:** The results show that multishearlets can neutralize the effect of noise in MRA images in a good way rather than shearlets. Moreover, the proposed scheme for segmentation can lead to 0.99 accuracy.

Keywords: *Active contour, COVID-19, high-pass filter, low-pass filter, multiwavelet, segmentation, shearlet transform*

Submitted: 27-Mar-2022 **Revised:** 18-Jun-2022 **Accepted:** 17-Aug-2022 **Published:** 12-Jul-2023

Introduction

Phylogenetic analysis of coronavirus offered that the coronavirus, severe acute respiratory syndrome coronavirus 2 (SARS-COV-2), originated in animals, perhaps in bats. It is transmitted to other animals and humans at the wet market of humans in Wuhan city. There is some proof that pangolin, a type of nocturnal anteater, imported this virus. Then this animal carries a coronavirus that is very similar to SARS-COV-2, but it is different in a crucial region, so it appoints viral infectivity and host range. Hence, the virus passed into humans; it spread so quickly from one person to another. Since coronavirus is more contagious, fast detection and isolation of affected people is crucial. A routine way for COVID-19 screening is medical imaging like X-ray or computed tomography (CT). By investigating X-ray or CT images, experts can detect the effects of coronavirus on each part of the body.[1,2]

The virus disrupts the lungs and can clot the blood and cause a heart attack. Another effect of this virus is its effect on the human brain that this virus may form air bubbles in the brain and affect the brain and its efficiency and memory. Hence, we must use brain magnetic resonance angiography (MRA) images to detect the effects of coronavirus on the brain. Since coronavirus can affect the brain, it can disrupt body's activities. Hence, investigating the brain during the infection of coronavirus infection is essential.[3-6]

By segmentation of the brain MRA image, affected regions from coronavirus

How to cite this article: Aghazadeh N, Moradi P, Noras P. Constructing multiwavelet-based shearlets and using them for automatic segmentation of noisy brain images affected by COVID-19. J Med Sign Sens 2023;13:183-90.

Address for correspondence:
Prof. Nasser Aghazadeh, Department of Applied Mathematics, Azarbaijan Shahid Madani University, Tabriz, Iran. E-mail: aghazadeh@azaruniv.ac.ir

Access this article online

Website: www.jmssjournal.net

DOI: 10.4103/jmss.jmss_29_22

Quick Response Code:

can be detected, and therefore, experts can determine affected regions fast by using machine learning methods in segmentation.[7,8] There are many classic and novel segmentation methods,[9-14] but, among them, the active contour is the most popular and fast.[15] Deep learning models demonstrated improved results, however, they are limited to the pixel-wise fitting of the segmentation map. This limitation can be tackled by considering the size of boundaries and the intensities inside and outside the region of interest during the learning process.[16-19]

This can be achieved by using an active contour loss function inspired by active contour model (ACMs). However, determining the initial curve plays a vital role in the segmentation of desired region.[20-23] If the initial curve is far from the region which we want to extract, the segmentation result will not be proper.[24-26] Therefore, here, we have used the image histogram for initial curve detection. It must be mentioned that, because the MRA images given by devices may have some noises, we have used a new idea for the first time for denoising based on shearlets constructed from multiwavelets.

Wavelets, because of their excellent localization and scalable properties, have been used in many applications. However, the limitation was that wavelets cannot detect curve-like singularities (such as edges) well and cannot detect the directions of the edges.[27,28] Nevertheless, shearlets[29-31] have been constructed in recent years to omit these limitations. Shearlets are constructed from wavelets by applying shear and scale operators on them.

We want to construct shearlets from multiwavelets.[32-34] In this way, we can extract features of the image better than one wavelet. Multiwavelets have wavelets that are symmetric and orthogonal simultaneously. Therefore, we have more freedom in using them rather than one wavelet, because wavelets do not have these properties simultaneously.

The rest of this paper is as follows: section 2 contains the advantages of multiwavelets and construction of multishearlets. In section 3, the proposed scheme for segmentation has been explained and some figures have been provided to show the results of using multishearlets for segmentation and denoising. In section 4, results of the proposed scheme have been discussed. Section 5 is conclusion and section 6 introduces the used dataset.

Materials

Advantage of multiwavelets

Wavelets which have developed since 1980 have many applications in signal and image processing, numerical analysis, approximation theory, data compression, and other fields. Wavelet theory is based on a refinement equation as follows:

$$\boldsymbol{\phi}(x) = \sqrt{2}\sum_{k} h_k \boldsymbol{\phi}(2x-k)\cdot \tag{1}$$

This relation defines the scale function ϕ. The scale function must satisfy multiresolution approximations (MRAs), and this leads to easy decomposition and reconstruction methods. There are some kinds of wavelets such as ridgelets and curvelets. One such generalization is multiwavelets. In multiwavelets, the scale function $\boldsymbol{\phi}$ is replaced by a vector.

$$\boldsymbol{\phi}(x) = \begin{pmatrix} \phi_1(x) \\ \vdots \\ \phi_r(x) \end{pmatrix} \tag{2}$$

which is called multiscale function, and the refinement equation is:

$$\boldsymbol{\phi}(x) = \sqrt{m}\sum_{k} h_k \boldsymbol{\phi}(2x-k) \tag{3}$$

Multiwavelets can affect to MRAs and fast algorithms just like scalar wavelets. However, they have some benefits:[28,35] first, they contain an extra degree of freedom, and this leads to some reducing restrictions in filter designing. For example, it is approved that a scalar wavelet cannot simultaneously have both orthogonality and asymmetric filters except the Haar scale function. Symmetric filters are necessary for symmetric signal expansion, while orthogonal filters lead to more accessible and more implement design. Moreover, the length and the number of vanishing moments depend directly on the filter length of scalar wavelets. Designing symmetric and orthogonal filters is impossible in the case of scalar wavelets. For example, the 4-tap Daubechies have an orthogonal filter and second order approximation, and the scaling function support is [0,3] but does not have the property of symmetry which is important. The filter of the biorthogonal 9/7 wavelet is symmetric, and this wavelet has a fourth order of approximation and support of scaling function is [0,9] but does not possess orthogonality.[36]

Legendre Multiwavelets

Here, we give an example of Legendre multiwavelets which is a linear multiwavelet.

Scaling functions

A pair of linear Legendre scaling functions on the interval [0,1] is defined as:

$$\begin{cases} \phi_0(x) = 1 & 0 \le x \le 1 \\ \phi_1(x) = \sqrt{3}(2x-1) & 0 \le x \le 1 \end{cases} \tag{4}$$

The integer translates of $\phi_0(x)$ and $\phi_1(x)$ together span V_0 in MRAs conditions and 1/2 scaled version of span V_1. Two-scale relation for them is:

$$\begin{bmatrix} \phi_0(x) \\ \phi_1(x) \end{bmatrix} = \begin{bmatrix} 1 & 0 & 1 & 0 \\ -\frac{\sqrt{3}}{2} & \frac{1}{2} & \frac{\sqrt{3}}{2} & \frac{1}{2} \end{bmatrix} \begin{bmatrix} \phi_0(2x) \\ \phi_1(2x) \\ \phi_0(2x-1) \\ \phi_1(2x-1) \end{bmatrix} \tag{5}$$

therefore, p (the low-pass matrix) is:

$$p=\begin{bmatrix}1 & 0 & 1 & 0\\ -\frac{\sqrt{3}}{2} & \frac{1}{2} & \frac{\sqrt{3}}{2} & \frac{1}{2}\end{bmatrix} \tag{6}$$

Wavelets

Corresponding to two scaling functions for linear Legendre multiwavelets, we have two wavelet functions as:

$$\psi_0(x)=\pm\begin{cases}-\sqrt{3}(4x-1) & 0\le x<\frac{1}{2}\\ +\sqrt{3}(4x-3) & \frac{1}{2}\le x<1\end{cases} \tag{7}$$

$$\psi_1(x)=\pm\begin{cases}6x-1 & 0\le x<\frac{1}{2}\\ 6x-5 & \frac{1}{2}\le x<1\end{cases} \tag{8}$$

and two-scale relation for these wavelets is as:

$$\begin{bmatrix}\psi_0(x)\\ \psi_1(x)\end{bmatrix}=\begin{bmatrix}0 & -1 & 0 & 1\\ \frac{1}{2} & \frac{\sqrt{3}}{2} & -\frac{1}{2} & \frac{\sqrt{3}}{2}\end{bmatrix}\begin{bmatrix}\phi_0(2x)\\ \phi_1(2x)\\ \phi_0(2x-1)\\ \phi_1(2x-1)\end{bmatrix}, \tag{9}$$

therefore, q (the high-pass matrix) is:

$$q=\begin{bmatrix}0 & -1 & 0 & 1\\ \frac{1}{2} & \frac{\sqrt{3}}{2} & -\frac{1}{2} & \frac{\sqrt{3}}{2}\end{bmatrix}. \tag{10}$$

Note that, each row of q is considered a high-pass filter.

Approximation order

We say that a multiscale function $\phi(t)$ has approximation order m if each polynomial $t^j, j=0,1,...,m-1$ is a linear combination of integer translates $\phi(t-k)$:[33]

$$t^j=\sum_{-\infty}^{\infty}y_k^{(j)}\,\phi(t-k),\ j=0,1,\cdots,m-1 \tag{11}$$

Suppose that $\phi(t)\in L^1$ and integer translates $\phi_j(t-k)$, $j=0,1,...,m-1$ are linearly independent. Then $\phi(t)$ provides approximation s if and only if L has eigenvalues $1, \frac{1}{2},\ldots,\left(\frac{1}{2}\right)^{s-1}$, where L is

$$L=\begin{bmatrix}\cdots & & & & & & & & \\ \cdots & H_3 & H_2 & H_1 & H_0 & & & & \\ & & \cdots & H_3 & H_2 & H_1 & H_0 & & \\ & & & & \cdots & H_3 & H_2 & H_1 & H_0\\ & & & & & & & & \cdots\end{bmatrix} \tag{12}$$

and H_i are low-pass matrices. In the case of Legendre multiwavelets, where we have H_0 and H_1 and other H_is are zero matrices. Then from Strang and Strla,[34] we can put L as

$$L=\begin{bmatrix}H_1 & H_0\\ [0]_{m\times m} & [0]_{m\times m}\end{bmatrix} \tag{13}$$

and it can be seen easily that if in Legendre multiwavelet has m scaling functions, then the accuracy order is m. For example, in the case of linear Legendre, if we put

$$L=\begin{bmatrix}1 & 0 & 1 & 0\\ -\frac{\sqrt{3}}{2} & \frac{1}{2} & \frac{\sqrt{3}}{2} & \frac{1}{2}\\ 0 & 0 & 0 & 0\\ 0 & 0 & 0 & 0\end{bmatrix} \tag{14}$$

we can see that its nonzero eigenvalues are 1, $\frac{1}{2}$.

Multiwavelets for image analysis

In 2*D* signals (images), we can use a multiwavelet filter bank for analyzing the image as shown in Figure 1. one must consider that each of H or G contains filters more than one.

Suppose that our image is represented by I_0 which is as an N by N matrix. The first step is to convolve all the rows by the row filters, where the first half of each row contains coefficients that belong to the first scaling function and the second half belongs to the second scaling function, and stores the result as a square array I_1. The next operation is the convolution of the columns of the array I_1 with a column filter where the first half of each column belongs to coefficients of the first scaling function and the second half of each column corresponds to the second scaling function and produces an output matrix I_2, such that the multiwavelet cascade begins with iterative filtering by low and highpass filters in horizontal and vertical directions. The result after one cascade step can be represented by:

$$\begin{bmatrix}L_1L_1 & L_2L_1 & H_1L_1 & H_2L_1\\ L_1L_1 & L_2L_2 & H_1L_2 & H_2L_2\\ \\ L_1H_1 & L_2H_1 & H_1H_1 & H_2H_1\\ L_1H_2 & L_2H_2 & H_1H_2 & H_2H_2\end{bmatrix} \tag{15}$$

Here, a typical block H_2L_1 contains low-pass coefficients corresponding to the first scaling function in the horizontal direction and highpass coefficients corresponding to the second wavelet in the vertical direction. The next step of the cascade will decompose the "low-pass" submatrix

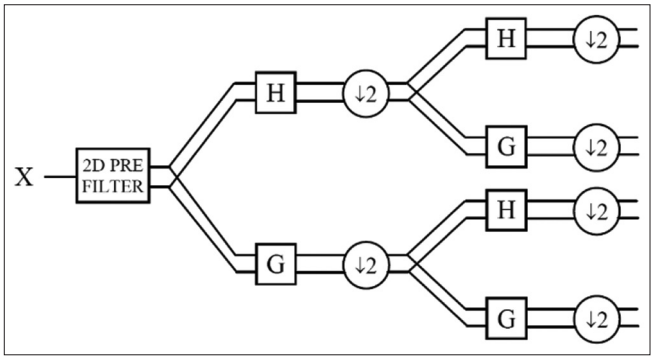

Figure 1: Analysis multiwavelet filter bank

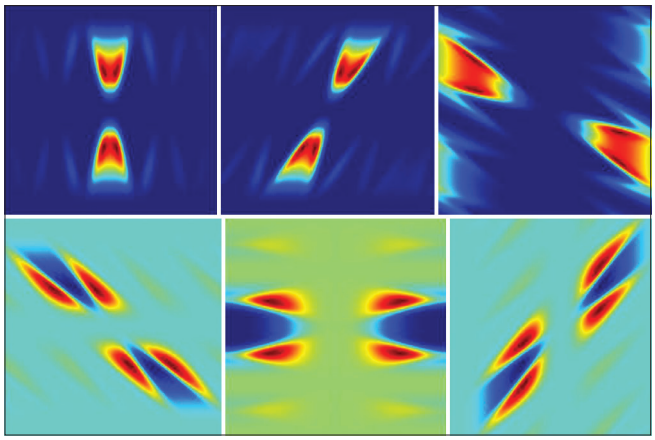

Figure 2: Some multishearlets for Legendre of order 3. The first row is for one wavelet and the second row is for another wavelet.

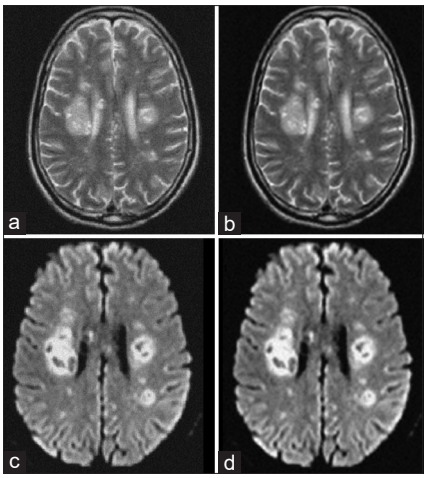

Figure 3: (a and c) Noisy image with Gaussian noise for σ = 10 (b and d) Denoising result by Multishearlets

L_1L_1 L_2L_1
L_1L_2 L_2L_2 in a similar manner.

Shearlets

If $\psi \in L^2(\mathbb{R}^2)$ satisfies

$$\int_{\mathbb{R}^2} \frac{\left|\widehat{\psi}(\xi_1,\xi_2)\right|^2}{\xi_1^2} d\xi_1 d\xi_2 < \infty \tag{16}$$

it can form an admissible shearlet. Note that any function Ψ where $\widehat{\psi}$ has compactly support far from the origin can be an admissible shearlet.[29] One example of these shearlets is given in the following definition. Let $\psi \in L^2(\mathbb{R}^2)$ be defined by

$$\widehat{\psi}(\boldsymbol{\xi}) = \widehat{\psi}(\xi_1,\xi_2) = \widehat{\psi}_1(\xi_1)\widehat{\psi}_2\left(\frac{\xi_2}{\xi_1}\right) \tag{17}$$

where $\Psi_1 \in L^2(R^2)$ is a discrete wavelet which satisfies the discrete Calderon condition by:

$$\sum_{j\in\mathbb{Z}} \left|\widehat{\psi}_1\left(2^{-j}\xi\right)\right|^2 = 1 \ \ for\ \xi \in \mathbb{R}, \tag{18}$$

with $\widehat{\psi}_1 \in C^{\infty}(\mathbb{R})$ and supp $\widehat{\psi}_1 \subseteq \left[\frac{-1}{2},\frac{-1}{16}\right] \cup \left[\frac{1}{2},\frac{1}{16}\right]$, and $\psi_2 \in L^2(\mathbb{R})$ is a bump function in the sense that

$$\sum_{k=-1}^{1} \left|\widehat{\psi}_2(\xi+k)\right|^2 = 1 \ \ for\ \xi \in [-1,1], \tag{19}$$

satisfying $\widehat{\psi}_2 \in C^{\infty}(\mathrm{R})$ and supp $\widehat{\psi}_2 \subseteq [-1,1]$. Therefore Ψ is called a classical shearlet. The classic shearlet is a Parseval frame for $L^2(\mathbb{R}^2)$. Therefore, the continuous shearlet system SH(Ψ) which is defined by

$$\mathrm{SH}(\psi) = \left\{\psi_{a,s,t} = T_t D_{A_a} D_{S_s}\psi : a > 0, s \in \mathbb{R}, t \in \mathbb{R}^2\right\} \tag{20}$$

where

$$A_a = \begin{pmatrix} a & 0 \\ 0 & a^{\frac{1}{2}} \end{pmatrix}, S_s = \begin{pmatrix} 1 & s \\ 0 & 1 \end{pmatrix}, T_t\psi(\mathrm{x}) = \psi(x-t), t \in \mathbb{R}^2, \tag{21}$$

can reproduce $L^2(\mathbb{R}^2)$. Let $\Psi \in L^2(R^2)$, the continuous shearlet transform of $f \in L^2(\mathbb{R}^2)$ is

$$f \in L^2\left(\mathbb{R}^2\right) \to SH_{\psi} f(a,s,t) = \langle f, \psi(a,s,t)\rangle, \tag{22}$$

associated with $a > 0$ as the scale variable, $s \in \mathbb{R}$ as the orientation variable and $t \in \mathbb{R}^2$ as the location variable. Cone-adapted shearlet systems have been designed to detect an edge along x_1 (horizontal edges) axis where a function is mainly concentrated along the ξ_2 axis in the frequency domain. In such cases, f can only be detected in the shearlet domain as $s \to \infty$ and it can be a severe limitation for some applications. For $\phi, \psi, \widehat{\psi} \in L^2\left(\mathbb{R}^2\right)$, the cone-adapted continuous shearlet system $SH(\phi,\psi,\widehat{\psi})$ is defined by

$$SH\left(\phi,\psi,\widetilde{\psi}\right) = \Phi(\phi) \cup \psi(\psi) \cup \widetilde{\psi}\left(\widetilde{\psi}\right), \tag{23}$$

where

$$\Phi(\phi) = \left\{\phi_t = \phi(.-t) : t \in \mathbb{R}^2\right\},$$

$$\psi(\psi) = \left\{\begin{array}{c} \psi_{a,s,t} = a^{\frac{-3}{4}}\psi\left(A_a^{-1}S_s^{-1}(.-t)\right) : a \in (0,1], \\ |s| < 1 + a^{\frac{1}{2}}, t \in \mathbb{R}^2 \end{array}\right\},$$

$$\psi(\widetilde{\psi}) = \left\{\begin{array}{c} \psi_{a,s,t} = a^{\frac{-3}{4}}\widetilde{\psi}(\widetilde{A}_a^{-1}S_s^{-\mathrm{T}}(.-\mathrm{t})) : a \in (0,1], \\ |s| < 1 + a^{\frac{1}{2}}, t \in \mathbb{R}^2 \end{array}\right\},$$

and $\tilde{A}_a = diag\left(a^{\frac{1}{2}}, a\right)$ and $\widetilde{\psi}(\xi_1,\xi_2) = \psi(\xi_2,\xi_1).\psi(\psi)$ is associated with horizontal cones and $\widetilde{\psi}(\widetilde{\psi})$ is associated with vertical cones.

Construction multishearlets based on multiwavelets

For designing multishearlets, each of $(\phi,\psi,\widetilde{\psi})$ in[34] is replaced by a vector function such as in (2). In Legendre

multiwavelets, even order wavelets are symmetric, that means $\psi\left(\mathrm{x}+\frac{1}{2}\right)=\psi\left(-x+\frac{1}{2}\right)$ and odd order wavelets are anti-symmetric, which means $\psi\left(\mathrm{x}+\frac{1}{2}\right)=-\psi\left(-x+\frac{1}{2}\right)$.[37,38] Therefore, in cone-adopted shearlets, the following equations will be satisfied for even order wavelets and odd order wavelets, respectively:

$$\psi\left(A_a^{-1}S_s^{-1}\left(.-\left(t+\begin{bmatrix}\frac{1}{2}\\ \frac{1}{2}\end{bmatrix}\right)\right)\right)=\psi\left(A_a^{-1}S_s^{-1}\left(.-\left(-t+\begin{bmatrix}\frac{1}{2}\\ \frac{1}{2}\end{bmatrix}\right)\right)\right) \quad (24)$$

$$\psi\left(A_a^{-1}S_s^{-1}\left(.-\left(t+\begin{bmatrix}\frac{1}{2}\\ \frac{1}{2}\end{bmatrix}\right)\right)\right)=-\psi\left(A_a^{-1}S_s^{-1}\left(.-\left(-t+\begin{bmatrix}\frac{1}{2}\\ \frac{1}{2}\end{bmatrix}\right)\right)\right). \quad (25)$$

Therefore, $\Psi_{a,s,t}$ will be symmetric for even order wavelets and anti-symmetric for odd order wavelets. These statements will be factual for $\Psi_{a,s,t}$ too. See some multishearlets in Figure 2.

First advantage of multishearlet

In multishearlets, we have symmetric shearlets, which are suitable for edge detection problems. Moreover, by increasing the order of wavelets in multiwavelet system, we can detect more singular points.

Second advantage of multishearlets: High approximation rate

Approximation rate of shearlets was $O(N^{-2}(logN)^3)$ and was proven in.[39] Approximation rate of using multishearlets is $O((Nk)^{-2}(logNk)^3)$, where k is the number of functions in multiwavelet system. If we substitute $\langle \mathrm{f},\psi_1\rangle+\ldots+\langle \mathrm{f},\psi_\mathrm{k}\rangle$ instead of $\langle \mathrm{f},\psi\rangle$ in proof of approximation rate in,[39] we can obtain the approximation rate of multishearlets. The critical equation for beginning the proof of approximation rate of multishearlets is $\langle \mathrm{f},\psi_1\rangle+\ldots+\langle \mathrm{f},\psi_\mathrm{k}\rangle\le k.2^{-\frac{3}{4}}$. Moreover, using multishearlets, instead of shearlets, has more freedom degree. In multishearlets, there is more than one wavelet, therefore we have more choices for our works. In denoising, smooth wavelets are effective and in edge detection sharp wavelets are effective.

Methods: Proposed scheme for segmentation

Step 1: Denoising Based on Multishearlets

Similar to denoising by shearlets with one shearlet generator, in denoising by multishearlets, we denoise the image by each of the shearlet generators and then we consider the mean image of these denoised results as a final denoised result. Note that in denoising, to get a good result, we can use a smooth multiwavelet and high order multiwavelet (see e.g. Figure 3).

In Tables 1 and 2, we have added Gaussian noise with different σ to the above images and then peak signal-to-noise ratio (PSNR) and Structural Similarity Index Measure (SSIM) values for each of the shearlet method and multishearlet method have been computed. These tables show the good performance of multishearlets, because multishearlets preserve structure better than shearlets and also the denoise image is more similar to shearlets resulting in the original image. *PSNR* and *SSIM* between the original image X and denoised image Y are defined as:

$$MSE=\frac{1}{mn}\sum_{i=1}^{m}\sum_{j=1}^{n}\left(X_{i,j}-Y_{i,j}\right)^2 \quad (26)$$

$$PSNR=10log_{10}\left(\frac{255^2}{\mathrm{MSE}}\right), \quad (27)$$

$$SSIM\left(X,Y\right)=\frac{\left(2\mu_x\mu_y+c_1\right)\left(2\sigma_{xy}+c_2\right)}{\left(\mu_x^2\mu_y^2+c_1\right)\left(\sigma_x^2+\sigma_y^2+c_2\right)} \quad (28)$$

Step 2: Histogram plotting of the image

Every image has intensity values between 0 and 255. When the image is normalized, these intensity values lie between 0 and 1. Histogram of the image gives us intensity information. Histogram of the image says how many pixels in the image have specific intensity values. Figure 4 shows the histogram of two brain images affected by coronavirus. By looking in these histograms and considering brain images, we can see peak in histograms that are related to regions affected by coronavirus. By considering regions that have intensity values in domain of this peak we can the boundary of regions that may be affected. Therefore, in using active contour for segmentation, the initial curve is determined automatically and hence the regions can be

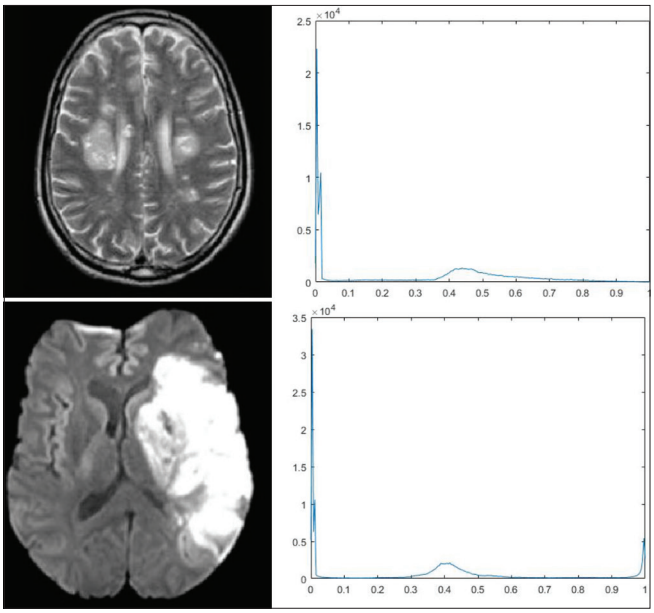

Figure 4: left column: brain images, right column: Histogram of the images in left column. Following figures show the results of segmentation by active contour on brain images by this scheme

segmented precisely. Segmentation algorithms are related to one of two fundamental properties of strength worthy's disconnectivity and similarity. The first one is partition of an image based on sudden changes in strength. The second category is based on partitioning one image in the areas that look like according to an earlier defined criterion. Histogram thresholding approach belongs to the second category. Histogram is created by splitting the data ranges in equal-sized bins. After that for every bin, the number of points from the data set. The data sets that fall in each bin are counted in thresholding foundation the gray level histogram matches with an image, combined of dark objects in a light background. Hence, objects and background pixels have gray levels grouped into two modes. A way to emerge the objects from the background is selecting a threshold ″T″. Any point (x, y) for $f(x, y) > T$ for is called a point of object on the other hand, the point is called a background.

Step 3: Segmentation by Active Contours

ACM or namely snakes proposed by Kass *et al*. is an applicable model in computer vision for delineating with object detection from the images which may have noise, also in shape recognition, segmentation, edge detection, and stereo matching.[35,40] Deformation of the snakes depends on the intensities and moves in a way that minimizes the energy inside and outside the snakes. A simple flexible snake is determined by a set of m points v_i for $i = 0,..., m-1$, the internal flexible energy term $E_{internal}$, and the external edge-based energy term $E_{external}$. The purpose of the internal energy term is to control the deformations made to the snake, and the purpose of the external energy term is to control the fitting of the contour onto the image. The external energy is usually a combination of the forces due to the image itself E_{image} and the constraint forces introduced by the user E_{cov}. By using ACM with initial curve which is extracted from the previous step, the brain images can be segmented.

Results and Discussion

The proposed scheme has been test on 70 images of whole brain atlas dataset. Tables 1 and 2 show that multishearlets have higher peak signal-to-noise ratio and SSIM values rather than shearlets in denoising. Moreover in Figure 5, we have presented the segmentation results on two sample images. The proposed method can reach to the accuracy of 0.99 and DSC of 0.97 in segmentation of the images. The results show that the proposed scheme can extract the region of tumor carefully.

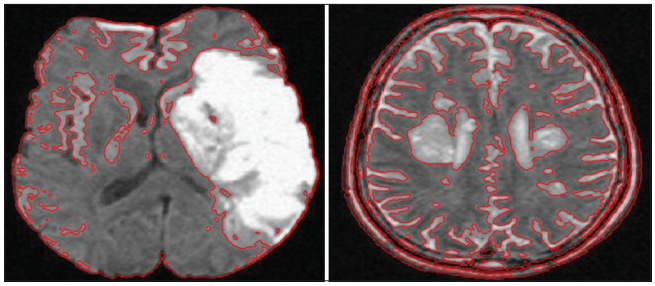

Figure 5: Result of the proposed scheme on 2 sample images

Conclusion

In this paper, we have designed multishearlets and have used them for denoising in brain images affected by coronavirus. Moreover, we have determined initial curve automatically based on histogram of the images. Then, we have applied active contour for segmentation of the affected regions. Experimental results demonstrated their good performance. Moreover, by using multiwavelets instead of wavelets in constructing of shearlets, we can extract features of the image by using smoother filter for smooth parts of the image and using sharper filter for sharp parts of the image. It can be an idea for segmentation by multishearlets.

Dataset

The data set which we have used is whole brain Atlas dataset http://www.harvard.edu/aanlib/home.html.

This dataset contains images of normal brain, brain attack, neoplastic disease or brain tumor, and inflammatory and Alzheimer images. These images are used in studying of brain diseases.

Financial support and sponsorship

None.

Table 1: Peak signal-to-noise ratio and structural similarity index measure comparison for first image

σ	PSNR		SSIM	
	Method			
	Shearlets	Multishearlets	Shearlets	Multishearlets
5	37.28	38.84	0.69	0.78
10	34.19	35.36	0.60	0.68
15	32.30	33.28	0.54	0.60
20	30.94	31.85	0.49	0.54
25	29.83	30.40	0.46	0.49

PSNR - Peak signal-to-noise ratio; SSIM - Structural similarity index measure

Table 2: Peak signal-to-noise ratio and structural similarity index measure comparison for second image

σ	PSNR		SSIM	
	Method			
	Shearlets	Multishearlets	Shearlets	Multishearlets
5	35.55	37.08	0.79	0.85
10	31.75	32.32	0.71	0.75
15	29.57	29.55	0.64	0.66
20	28.05	27.53	0.58	0.58
25	26.82	25.81	0.52	0.50

PSNR - Peak signal-to-noise ratio; SSIM - Structural similarity index measure

Conflicts of interest

There are no conflicts of interest.

References

1. Mohammadimajd E, Lotfinia I, Salahzadeh Z, Aghazadeh N, Noras P, Ghaderi F, *et al.* Comparison of lumbar segmental stabilization and general exercises on clinical and radiologic criteria in grade-I spondylolisthesis patients: A double-blind randomized controlled trial. Physiother Res Int 2020;25:e1843.
2. Moftian N, Hachesu PR, Pourfeizi HH, Samad-Soltani T, Aghazadeh N, Poureisa M, *et al*. Newfangled procedures using x-ray to determine the cobb angle in patients with scoliosis: An updated systematic review. Curr Med Imaging Rev 2019;15:922-2. doi: 10.2174/1573405614666180531073300.
3. Liu YC, Kuo RL, Shih SR. COVID-19: The first documented coronavirus pandemic in history. Biomed J 2020;43:328-33.
4. Gulko E, Oleksk ML, Gomes W, Ali S, Mehta H, Overby P, *et al.* MRI brain findings in 126 patients with COVID-19: Initial observations from a descriptive literature review. AJNR Am J Neuroradiol 2020;41:2199-203.
5. Lin E, Lantos JE, Strauss SB, Phillips CD, Campion TR Jr., Navi BB, *et al.* Brain imaging of patients with COVID-19: Findings at an academic institution during the height of the outbreak in New York City. AJNR Am J Neuroradiol 2020;41:2001-8.
6. Brown EE, Kumar S, Rajji TK, Pollock BG, Mulsant BH. Anticipating and mitigating the impact of the COVID-19 pandemic on Alzheimer's disease and related dementias. Am J Geriatr Psychiatry 2020;28:712-21.
7. Ronneberger O, Fischer P, Brox T. U-net: Convolutional networks for biomedical image segmentation, International Conference on Medical Image Computing and Computer-Assisted Intervention. (MICCAI 2015): : Springer; 2015. p. 234-41.
8. Ding K, Xiao L, Weng G. Active contours driven by region-scalable fitting and optimized laplacian of gaussian energy for image segmentation. Signal Process 2017;134:224-33.
9. Mirzafam M, Aghazadeh N. A three-stage shearlet-based algorithm for vessel segmentation in medical imaging. Pattern Anal Appl 2021;24:591-610.
10. Siadat M, Aghazadeh N, Akbarifard F, Brismar H, Oktem O. Joint image deconvolution and separation using mixed dictionaries. IEEE Trans Image Process 2019;28:3936-45.
11. Sharafyan-Cigaroudy L, Aghazadeh N. A new multiphase segmentation method using eigenvectors based on *k* real numbers. Circuits Syst Signal Process 2017;36:1445-54.
12. Sharafyan-Cigaroudy L, Aghazadeh N. A multiphase segmentation method based on binary segmentation method for gaussian noisy image. Signal Image Video Process 2017;11:825-31.
13. Aghazadeh N, Akbarifard F, Sharafyan-Cigaroudy L. A restoration-segmentation algorithm based on flexible Arnoldi-Tikhonov method and curvelet denoising. Signal, Image and Video Processing 2016;10:935-42.
14. Sharafyan-Cigaroudy L, Aghazadeh N. A Binary-Segmentation Algorithm Based on Shearlet Transform and Eigenvectors. 2nd International Conference on Pattern Regonition and Image Analysis (IPRIA); [Doi: 10.1109/PRIA.2015.7161618].
15. Wu B, Yang Y. Local-and Global-Statistical-Based Active Contour Model for Image Segmentation, Mathematical Problems in Engineering; 2012.
16. Cheng D, Liao R, Fidler S, Urtasun R. Darnet: Deep active ray network for building segmentation. In: Proceedings of the IEEE Conference on Computer Vision and Pattern Recognition. (CVPR): 2019. p. 7431-9.
17. Badrinarayanan V, Kendall A, Cipolla R. SegNet: A deep convolutional encoder-decoder architecture for image segmentation. IEEE Trans Pattern Anal Mach Intell 2017;39:2481-95.
18. Haque IR, Neubert J. Deep learning approaches to biomedical image segmentation. Inform Med Unlocked 2020;18:100297.
19. Sultana F, Sufian A, Dutta P. Evolution of image segmentation using deep convolutional neural network: A survey. ArXiv:2001.04074v3.
20. Ding K, Xiao L. A simple method to improve initialization robustness for active contours driven by local region fitting energy. ArXiv: 1802.10437v2.
21. Memon AA, Soomro S, Shahid MT, Munir A, Niaz A, Choi KN. Segmentation of Intensity-Corrupted Medical Images Using Adaptive Weight-Based Hybrid Active Contours. Comput Math Methods Med 2020;2020:6317415.
22. Lio G,, Dong Y, Deng M, Liu Y. . Magnetostatic Active Contour Model with Classification Method of Sparse Representation. J Electr Comput Eng 2020; 5438763.
23. Ali H, Sher A, Saeed M, Rada L, . Active contour image segmentation model with de-hazing constraints. IET Image Process 2020;14:921-8.
24. Menon RV, Kalipatnapu S, Chakrabarti I. High Speed VLSI Architecture for Improved Region Based Active Contour Segmentation Technique; March, 2021.
25. Zhang Y, Duan J, Guo Y. Multi-Atlas Based Adaptive Active Contour Model with Application to Organs at Risk Segmentation in Brain MR Images; October, 2020.
26. Fang J, Liu H, Liu H. Region-Edge-Based Active Contours Driven by Hybrid and Local Fuzzy Region-Based Energy for Image Segmentation; February, 2021.
27. Noras P, Aghazadeh N. Directional schemes for edge detection based on B-spline wavelets. Circuits, Systems, and Signal Processing 2018;37:3973-94.
28. Aghazadeh N, Gholizade-atani Y, Edge detection with hessian matrix property based on wavelet transform. J Sci Islam Repub Iran 2015;26:163-70.
29. Kutyniok G, Lim WQ, Steidl G. Shearlets: Theoty and Applications. Gamm-Mitteilungen. 2014;37:259-80. https://doi.org/10.1002/gamm.201410012.
30. Kutyniok G, Labate D. Introduction to shearlets. In: Kutyniok G, Labate D, editors. Shearlets: Applied and Numerical Harmonic Analysis. Boston: BirkhÃ¤user; 2012.
31. Reisenhofer R, Kiefer J, King EJ. Shearlet-based detection of flame fronts. Exp Fluids 2016;57:41.
32. Soman NG, Ramachandran KP, Resmi KI. Insight Into Wavelets: From Theory to Practice. 3rd ed. PHI Learning; 2010.
33. Strla V. Multiwavelets: Theory and Applications, Massachusetts Institue of Technology; 1996.
34. Strang G, Strla V. Multiwavelets: Orthogonal Multiwavelets with Vanishing Moments, Massachusetts Institue of Technology; Cambridge MA 02139.
35. Kass M, Witkin A, Terzopoulos D. Snakes: Active contour models. Int J Comput Vision 1988;1:321-31.
36. Kenny G, Mallon PW. COVID19- clinical presentation and therapeutic considerations. Biochem Biophys Res Commun 2021;538:125-31.
37. Parra CM, Gupta M, Mikalef P. Information and Communication Technologies (ICT)-Enabled Severe Moral Communities and How the (Covid19) Pandemic Might Bring New Ones; November, 2020.

38. Berretta AA, Silveira MA, Cóndor Capcha JM, De Jong D. Propolis and its potential against SARS-CoV-2 infection mechanisms and COVID-19 disease: Running title: Propolis against SARS-CoV-2 infection and COVID-19. Biomed Pharmacother 2020;131:110622.
39. Kutyniok G, Lim WQ, Compactly supported shearlets are optimally sparse. J Approximation Theory 2011;163:1564-89.
40. Jiangxiong F, Huaxiang L, Hesheng L. Fuzzy Region-Based Active Contour Driven by Global and Local Fitting Energy for Image Segmentation; December, 2020.